

All-in-All: Dead Lithium-Ion Battery to Active Lithium-Ion Capacitor

Akshay Manohar,^[a] Aranganathan Viswanathan,^[a] Yun-Sung Lee,^{*,[b]} and Vanchiappan Aravindan^{*,[a]}

Here, we have developed lithium-ion capacitors (LICs) with all the components, except the electrolyte solution, effectively recycled from the spent Lithium-ion batteries (LIBs). Hybrid capacitors, such as LICs, are potential breakthroughs in electrochemical energy storage devices, where most research is focused. These devices can simultaneously guarantee high energy and power by hybridizing battery-type and capacitive-type electrodes with two different reaction mechanisms. We have successfully upcycled the graphite, current collector, separator, etc., from the spent LIBs to fabricate a high-performance LIC. Our LIC consists of recovered graphite (RG) coated over recovered copper foil as an anode, recycled polypropylene as the separator, and reduced graphene oxide (rGO) synthe-

sized from RG as the cathode. The RG half-cell exhibited an excellent specific capacity of 302 mAh g⁻¹ even after 75 charge-discharge cycles with a coulombic efficiency of >99%. The Li/rGO displayed remarkable cycling performance for over 1000 cycles with high stability and reversibility. Subsequently, the pre-lithiated RG (p-RG) electrode is paired with the rGO electrode under the balanced loading conditions to construct LIC, rGO/p-RG, delivering a maximum energy density of 185 Wh kg⁻¹ with ultra-long durability of more than 10,000 cycles. The possibility of LIC under different climatic conditions is also explored, and its remarkable performance under various temperature conditions is worth mentioning.

Introduction

The 21st century is experiencing a drastic transition of energy storage from fossil fuels to electrochemical energy storage. Batteries and Supercapacitors are in great demand with the increased use of electrical and electrochemical energy storage devices. All these started with Sony commercializing the first Lithium-ion battery (LIB) in the early 1990s.^[1–3] However, we are still in the infant stage of energy gathering rather than energy farmers. Research and development for the most modern electrochemical devices are increasing, whereas the exploitation of conventional devices is at its peak. As a result, the piling up of spent devices goes hand in hand with the usage. The growing population and advancement of technology lead to increased demand for these devices, resulting in the massive generation of waste. In this short period, a tremendous amount of waste has been generated, and it will hit 11 million tons by 2030 globally.^[4] In addition, the limited sources of raw materials are a severe concern when considering the long run of these electrochemical energy storage devices. Hence, an urgent call

arises to recover the spent batteries in the most eco-friendly and economical way to efficiently utilize new devices for sustainable development.^[5–11]

In general, LIBs consist of graphite coated over a copper current collector as an anode, lithiated compounds (LiCoO₂, LiNi_xMn_yCo_zO₂, LiFePO₄, LiMn₂O₄, etc.) coated over the aluminium foil as cathode and where these two electrodes physically separated by a polypropylene separator.^[12] Most people are interested in recovering the valuable elements from the cathodes of spent LIBs, and many efforts are being put into its efficient separation. The graphite, current collectors, and separators are the least priority from the recycling perspective, though they can be recycled more efficiently using simple methods. Graphite, as we all know, is the finest and most high-performance anode material, which is unbeaten even after 33 years of commercialization in LIBs. Moreover, 12 to 21 wt% of the LIBs are occupied by graphite, which is a significant composition in the battery components. Copper foil is also another valuable material (\$ 640 per m², for 20 μm thickness and >99% purity), which can bring a better economic benefit to recycling. Polypropylene separators are widely used in LIBs, and reports on its recovery are very rare. These are burdens for the environment as they fill the land and take many years to decompose. Therefore, our group is actively involved in recycling graphite,^[13–18] copper current collector,^[4,8,19] and separators^[20–22] to upcycle as the component for batteries and capacitors, which is significant and indispensable for sustainable development.

There are various reports on battery recycling and re-utilisation of the materials in metal-ion batteries and capacitors. Akshay *et al.*^[23] recovered copper foil from spent LIBs and transferred it to CuO for using as the conversion-type anode for

[a] Department of Chemistry, Indian Institute of Science Education and Research (IISER), Tirupati, India

[b] School of Chemical Engineering, Chonnam National University, Gwang-ju, Republic of Korea

Correspondence: Vanchiappan Aravindan, Department of Chemistry, Indian Institute of Science Education and Research (IISER), Tirupati 517619, India. Email: Aravind_van@yahoo.com

Yun-Sung Lee, School of Chemical Engineering, Chonnam National University, Gwang-ju 61186, Republic of Korea. Email: leeys@chonnam.ac.kr

Supporting Information for this article is available on the WWW under <https://doi.org/10.1002/cssc.202400449>

the fabrication of LIC. As mentioned, our group has also recovered graphite and separators and used them as components in batteries^[24] and supercapacitors.^[25] Bhattacharjee *et al.*^[26] utilized recovered graphite as a source for both anode and cathode of LIC. They used graphite-graphene composite and surface-activated recycled graphene as the cathode. The cathode materials are of great interest, as we discussed above. Natarajan *et al.*^[27] regenerated the MnCO_3 cuboids from the spent LIB cathode and utilized it as the anode for LIC. Most of those works use recycled materials in a small percentage of their devices. Here, our work becomes completely unique from the previous reports. We have fabricated an LIC with all the components, except the electrolyte, recovered from the spent LIBs. LICs, as we know, can provide energy and power simultaneously in a single system.^[28–31] It has a battery-type anode that undergoes faradaic reactions and a capacitive-type cathode that undergoes non-faradaic adsorption/desorption processes. Our anode is recovered graphite (RG) coated over the recovered copper foil, the cathode is the reduced graphene oxide (rGO) synthesized from RG using modified Hummer's method, and the separator is the recovered polypropylene. We have explored all the possibilities of recovering these materials in the most efficient and eco-friendly way to obtain high-purity materials. The electrochemical performances of these materials are studied in half-cell and full-cell assemblies, where the superior performance was displayed in terms of energy density, power density, cyclability, and stability to various temperature conditions are discussed in detail.

Result and Discussion

A detailed explanation of the recovery of valuable materials (graphite, current collector, and separator) and their regeneration in the LIC is discussed in the experimental section. X-ray diffraction studies are used to examine the recovered material's purity and crystallographic structure. The sharp peak of recovered graphite (Figure 1a, olive colour) is positioned at 26.5° , and all the other peaks match the graphite's standard data (DB Card Number: 04–014–0362). The graphite exhibits a hexagonal crystal structure with unit cell parameters $a=b=2.464 \text{ \AA}$, $c=6.736 \text{ \AA}$; $\alpha=90^\circ$, $\beta=90^\circ$, $\gamma=120^\circ$ and belongs to 194: P63/mmc space group. The peak at 26.5° corresponds to the hkl plane (002), and the inter-graphene layer spacing is about 3.3 \AA . In addition, the particle size of the RG was calculated using the Debye Scherrer formula (given below) and is found to be $\sim 2.8 \text{ nm}$.

$$D = \frac{0.9\lambda}{\beta \cos \theta}$$

Where λ is the X-ray wavelength, β is the full width at half maximum (FWHM, in radians), and θ is the Braggs angle (in radians). The rGO displays broad peaks (Figure 1a, blue colour), positioned at $2\theta = 25, 43$, and 78.5° , indicating the amorphous nature of the material. Also, these peaks match the previous reports,^[32] and no additional peaks are present, confirming the absence of impurity.

The texture and surface of both RG and rGO were inspected from the nitrogen adsorption/desorption studies in Figure S1. As expected, the rGO has a high surface of $295 \text{ m}^2 \text{ g}^{-1}$ with a

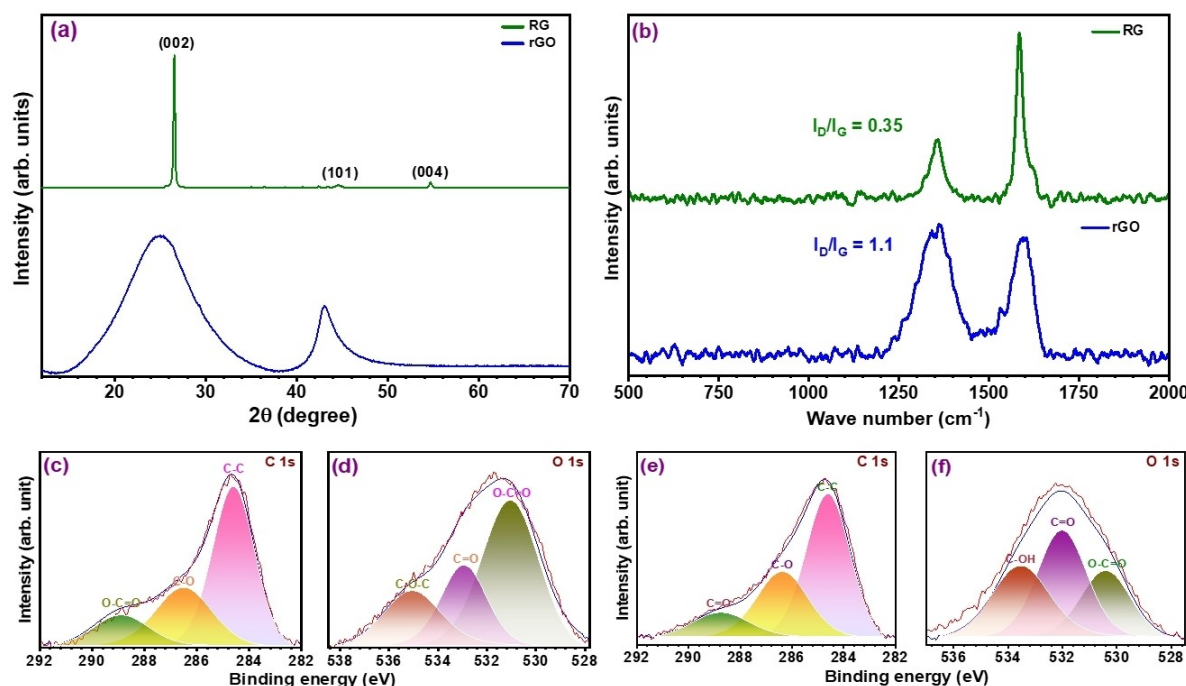


Figure 1. Physical characterizations: (a) XRD pattern of RG and rGO, (b) Raman spectra of RG and rGO, (c & d) deconvoluted XPS spectra of RG, and (e & f) deconvoluted XPS spectra of rGO.

pore radius of 14.8 Å and a pore volume of 0.17 cc g⁻¹. On the other hand, the RG has a surface area of 14.8 m² g⁻¹ with pore radius and pore volume of 16.9 Å and 0.058 cc g⁻¹, respectively. Raman spectra of RG (green) and rGO (blue) are given in Figure 1b. In the case of RG, the spectra display sharp peaks at ~1359 and ~1584 cm⁻¹, representing the D and G bands, respectively. The D-band or defect/dispersive band corresponds to the structural defect on graphite due to the continuous cycling of the LIB. On the other hand, the G band corresponds to the in-plane stretching of the sp² carbon atoms.^[25] The degree of graphitization is also calculated from the intensity ratio of D and G band peaks (I_D/I_G) and is found to be 0.35. For rGO, two vibrational bands are present at 1361 and 1604 cm⁻¹, representing the D and G bands, respectively, and the I_D/I_G ratio value from peaks is calculated to be 1.1. The value of rGO seems to be higher than RG, indicating the higher disorderness/discontinuity in the graphene layers.

The elements present at the surface of RG/rGO were examined from the XPS survey, and they consist of peaks corresponding to C (carbon) and O (oxygen). The RG XPS spectrum of C 1s (Figure 1c) has three deconvoluted peaks at 284.6, 286.5, and 288.9 eV, corresponding to C–C, C–O, and O–C=O bonds, respectively. The O 1s is also deconvoluted to three peaks at 531, 532.9, and 535 eV, representing O–C=O, C=O, and C–O–C, respectively (Figure 1d). The C 1s spectrum of rGO (Figure 1e) is split into three peaks corresponding to C–C, C–O, and C=O bonds positioned at 284.6, 286.4, and 288.7 eV, respectively. The peaks representing O–C=O, C=O, and C–OH bonds can be observed from the O 1s spectrum at

binding energies 530.4, 532, and 533.5 eV, respectively (Figure 1f).^[33]

The surface morphology of all the recovered materials at different magnifications is given in Figure 2. The flaky morphology of graphite can be observed from Figure 2(a, b). The rGO, on the other hand, has a wavy sheet-like structure observed from the different magnification images (Figure 2(c, d)). The morphology of the recycled separator (RS, Figure 2(e, f)) is also compared with the Celgard PP/PE/PP trilayer separator (Figure S2 (a, b)), where the increase in pore size could be observed as a result of the continuous cycling. In addition, the cross-section images of the RG electrode were also taken at different magnifications and are given in Figure 2g, Figure S2 (c–e). The cross-sectional EDS mapping of the RG electrode displays the distribution of carbon (graphite) and copper from the current collector (Figure 2h). The elemental distribution of RG and rGO is evident from the EDS elemental mapping study given in Figure 2 (i–k), where the C:O ratio of rGO is found to be 8.42:1.58.

Electrolyte Studies

Electrolytes are crucial to any electrochemical power source, especially LIC, which significantly determines its electrochemical performance. We have performed a few studies on how electrolytes can contribute to the better performance of LICs. Initially, the compatibility of the electrolyte with the separator was examined using an ion-blocking cell. The EIS studies were performed for the cell with 1 M LiPF₆ in EC: DMC (1:1) as the

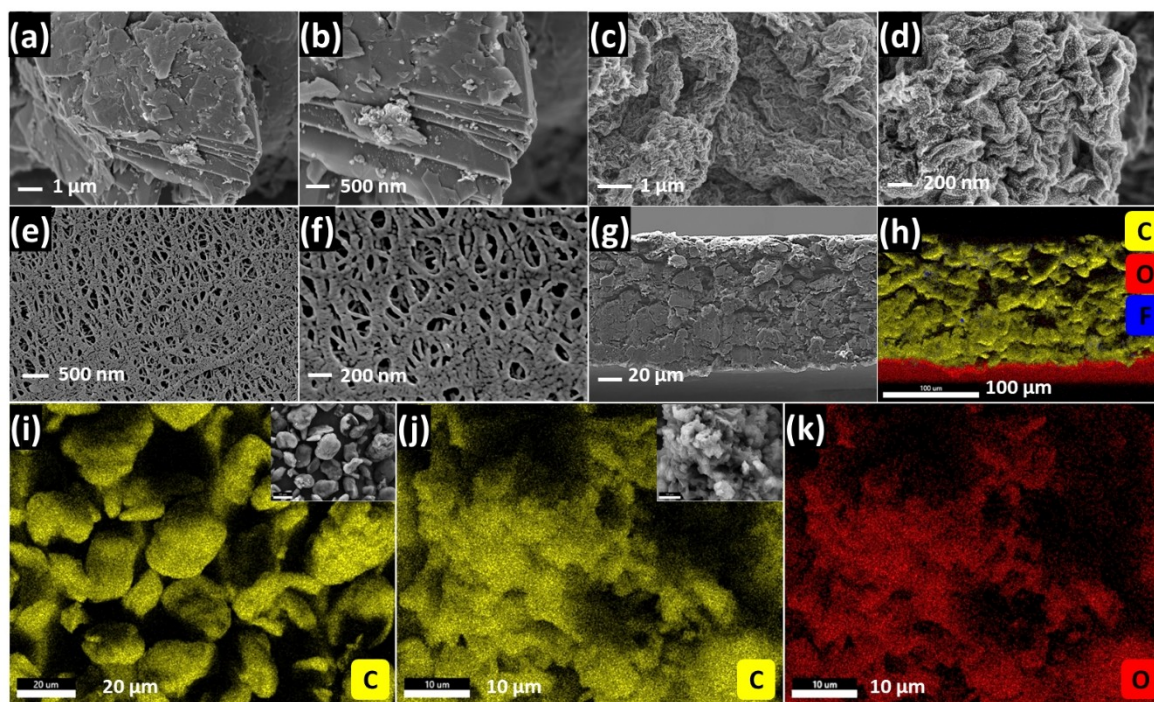


Figure 2. (a–f) FE-SEM images at different magnifications: RG (a, b), rGO (c, d), and recovered polypropylene separator (e, f), and a cross-section of RG electrode (g). Elemental mapping of RG electrode cross-section (h), RG (i), and rGO (j, k).

electrolyte for FS/RS at various temperatures ranging from 0–60 °C. Ionic conductance vs. $1000/T$ was plotted for both separators, as shown in Figure 3a. The activation energy was obtained from the slope of the curve using the Arrhenius equation given below:

$$\sigma = \sigma_0 e^{-E_a/RT}$$

where σ , σ_0 , E_a , R , and T are ionic conductivity, absolute conductivity, activation energy, universal gas constant, and temperature, respectively. The activation energies of the cells with FS and RS are calculated to be 18.5 and 15.5 kJ mol^{−1}, respectively.^[21] The ionic conductivity value of both separators was obtained from the ionic conductivity vs. inverse temperature plot given in Figure S3 (a). The similar order value of $\sim 10^{-4}$ S cm^{−1} for FS and RS proves that both the separators provide a similar kind of transportation of Li-ions through their porous structure.

The stability of the electrolyte at high voltage is tested using the linear sweep voltammetry (LSV) technique, where the cell was tested from the open circuit voltage (OCV) to 6 V vs. Li

at a slow scan rate of 0.1 mV s^{−1}. For both the cells with FS and RS, the electrolyte decomposition started from 4.1 V vs. Li, which can be observed clearly from the peaks given in Figure 3b. In addition, the electrolyte's stability and the quality of RS can be inferred from this study, as the change in the separator does not affect the electrolyte's performance.

Separator Studies

Mechanical performance, such as tensile strength, is an important parameter related to the safety of the separator as it should be able to withstand several mechanical stresses, such as lithium dendrite growth, that lead to short circuits and battery failure.^[12] As expected, the RS could reach only up to a maximum tensile strength of ~ 128 MPa, slightly lower than that of the fresh separator (FS, ~ 178 MPa). This low mechanical strength is mainly because of the large number of ionic transports it has undergone. However, the tensile strain of both FS and RS was found to be almost similar, which explains the

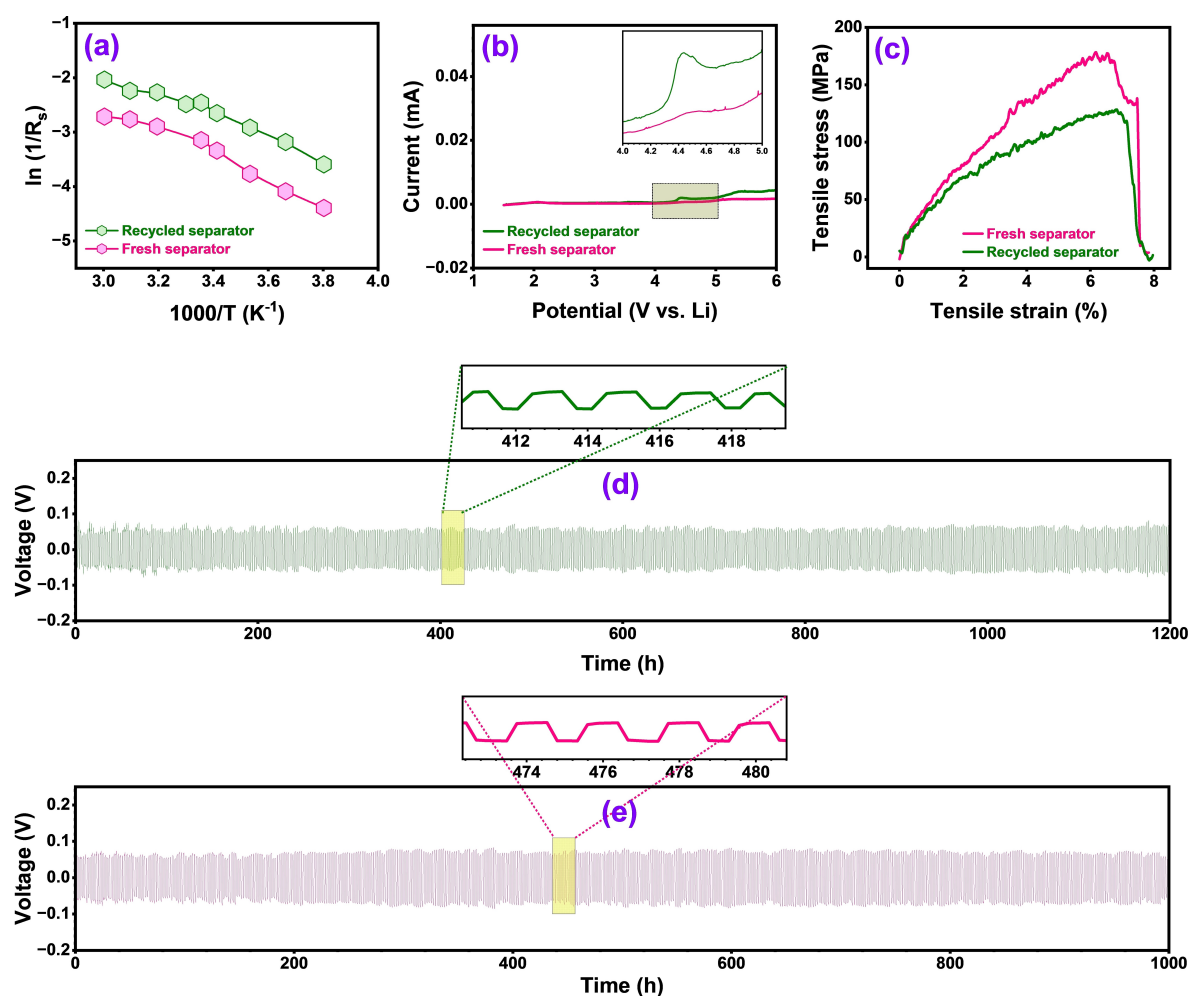


Figure 3. (a) Arrhenius plot for ion-blocking cell with 1 M LiPF₆ in EC:DMC (1:1) of fresh (pink) and used (olive) separator, (b) linear sweep voltammetry of Li/Stainless steel asymmetric cell with both fresh (pink) and used (olive) separator, (c) tensile stress vs. strain plot of fresh (pink) and used (olive) separator, Li-plating-stripping GCD test of Li/Li symmetric cell with: (d) recycled (RS), and (e) fresh separator (FS).

good mechanical strain of the recycled separator we used in LIC.

The contact angle of both the FS and RS were also measured to analyze the wettability (Figure S2 (g, h)). A drop of electrolyte is placed over the separator (FS/RS), and the image is captured using the instrument. The contact angle of the electrolyte droplet is measured using the ImageJ software, and it is found that the RS (25.7°) has a lower contact angle than the fresh one (50.4°). Hence, it has more wettability, which can be mainly because of the cycling it has undergone or could be due to the difference in the manufacturing process. The better wettability of RS improved the ionic conductivity and, thereby, the overall electrochemical performance of the LIC.

Figure S3(b) compares the electrolyte uptake behaviour of both fresh and used separators, as it is a significant physical property that affects the electrochemical performance of LICs. The separator should be able to absorb a sufficient amount of electrolyte during the cycling process so as to reduce the impedance in ionic transport.^[20] Both the separators were soaked in the electrolyte (1 M LiPF₆ in EC: DMC (1:1)), and the uptake by each was measured in regular intervals up to 1 h. The recycled separator has an electrolyte uptake from 621 to 1648% when time is increased from 1 min. to 1 h, whereas the fresh one has only a 193 to 304% increase. This excellent electrolyte uptake of recycled separator eventually improves the ionic conductivity, power density, and, therefore, the overall performance of the LIC. The significant difference in uptake values of separators also opens the door to using recycled separators in commercial LIBs and LICs, replacing the existing fresh ones. This uptake difference of separators could be due to various reasons, including the manufacturing process, material, no. of cycling, etc. However, recycled ones are a much better option for use in LICs from a second-life point of view.

The integrity and robustness of the separators were further studied from the lithium stripping-plating GCD analysis using the Li/Li symmetric cell (Figure 3 (d, e)). The cells with FS and RS were subjected to cycling at a current of 0.1 mA cm⁻² with a capacity limit of 0.1 mAh g⁻¹. The RS-based cell exhibited cycling for more than 1200 hours, whereas the FS-based cell cycling was limited to 1000 hours. Both the cells exhibited polarisation after subsequent cycling. In the initial cycles, the voltage for both the FS and RS-based cells was 50 mV. Nevertheless, after 1000 h, the voltage rises to 60 mV for the FS-based one. However, for the RS-based cell, the change in voltage of 60 mV happened only after 1200 h. This clearly explains the integrity of RS for long cycling without causing any failure.

Electrochemical Performance of RG and rGO

The electrochemical performance exhibited by the RG was examined from the cyclic voltammetric (CV), potentiostatic electrochemical impedance spectroscopy, and galvanostatic charge-discharge (GCD) studies. The RG coated over the recovered copper foil was used as the electrode, and the half-cell performances were evaluated by pairing this electrode with the lithium metal. The Li/RG half-cell was subjected to CV

studies between 0.005 to 2.5 V vs. Li at a scan rate of 0.1 mV s⁻¹ (Figure 4a). The CV traces display two broad cathodic peaks at 1.3 and 0.64 V vs. Li, indicating the solid electrolyte interphase (SEI) layer formation as a result of the decomposition of the electrolyte solution. These peaks are absent in the following cycles as the SEI formation happens predominantly in the first discharge, and the formed layer is stable. We could also observe characteristic cathodic peaks at 0.15 and 0.05 V vs. Li of graphite, indicating the intercalation of Li⁺ (LiC₆) via the staging process.^[34] The sharp anodic peak at 0.26 V vs. Li displays the reversible reaction, the deintercalation of Li⁺ ions from the graphite intercalated compound, LiC₆. The cathodic peaks at the higher potential in the first cycles were found to be absent in the following cycles, indicating that the SEI layer formed barriers to the contact between the electrode and electrolytes, thereby preventing further electrolyte decomposition.

Figure 4b displays the 1st, 10th, 25th, and 50th GCD curves of the RG electrode at a current density of 0.1 A g⁻¹. As observed in the CV curve, the initial discharge of the Li/RG half-cell has a plateau at 0.64 V vs. Li, replicating the SEI layer formation, which is commonly observed for graphitic anodes. In addition, this plateau is absent for the following cycles, which agree with the CV results. The CV was also performed at different scan rates (0.1 to 1 mV s⁻¹), which is given in Figure S4 (a). The diffusion coefficient was also calculated from it using the Randles-Sevcik equation given below:

$$I_p = 2.69 \times 10^5 \times n^{3/2} \times AC (Dv)^{1/2}$$

Where I_p is the current maximum, n is the no. of electrons transferred during the redox reaction, A is the area of the electrode, C is the concentration in mol cm⁻³, D is the diffusion coefficient in cm² s⁻¹, and v is the scan rate. Re-arranging the above equation, the diffusion coefficient can be calculated from the slope of I_p vs. $v^{1/2}$ plot (Figure S4 (b)). The obtained diffusion coefficient for anodic and cathodic peaks are 2.49×10^{-11} and 8.16×10^{-11} cm² s⁻¹, respectively.

The Li/RG half-cell has an initial discharge capacity of 408 mAh g⁻¹ and a charge capacity of 355 mAh g⁻¹ with a high coulombic efficiency of 87%. The initial loss in capacity observed in graphitic anodes is due to the lithium-ion consumption for the SEI layer formation, which is explained by the CV results. As the cycle progressed, there was not much drop in the specific capacity, and the RG maintained a discharge capacity of 302 mAh g⁻¹ after 75 cycles, as observed in Figure 4d. Also, the coulombic efficiency value increased after the first cycle and maintained a value close to 100% till the 80th cycle, which displays the RG electrode's excellent reversibility. The rGO electrode paired with Li metal was initially subjected to cyclic voltammetric studies between 1.5 to 4.5 V vs. Li at different scan rates (1 to 10 mV s⁻¹), as given in Figure S5. In the GCD analysis (Figure 4c) of the half-cell at a current density of 0.1 A g⁻¹ with the progression in cycles, the coulombic efficiency value is reduced to nearly 100% and was almost stable for 1000 cycles. The Li/rGO half-cell also retained a specific capacity of 74 mAh g⁻¹ even after 1000 charge-discharge cycles with high coulombic efficiency (Figure 4e).

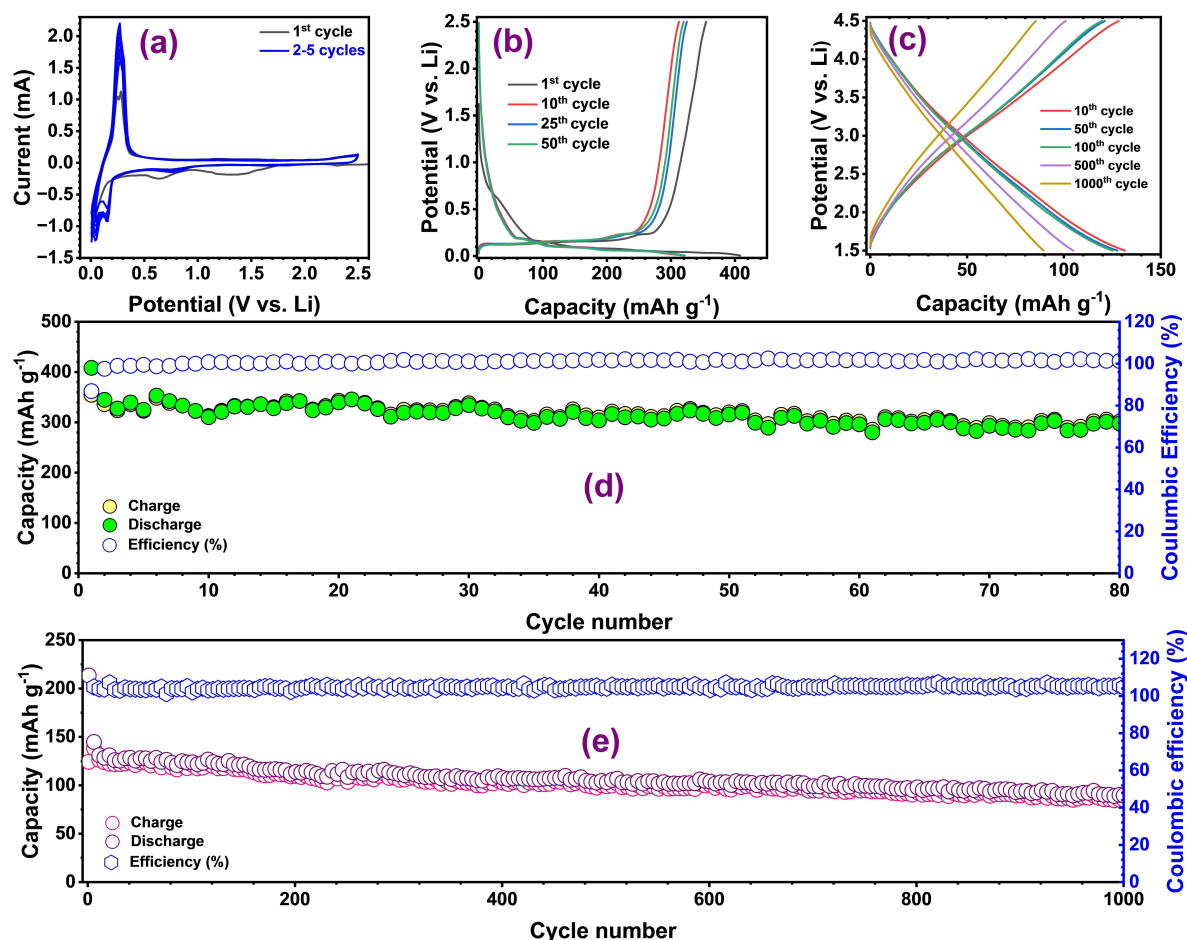


Figure 4. Electrochemical performance of RG and rGO in half-cell configuration: (a) Cyclic voltammogram of RG, (b) typical galvanostatic charge-discharge curve of RG (1st, 10th, 25th, and 50th cycles) at a current density of 0.1 A g⁻¹, (c) typical galvanostatic charge-discharge of rGO (10th, 50th, 100th, 500th and 1000th cycles) at a current density of 0.1 A g⁻¹, (d) capacity vs. cycle number plot of RG, and (e) GCD cycling profile of rGO at 0.1 A g⁻¹ current density.

A stable and robust solid electrolyte interface (SEI) layer has many things to do with the performance of the LIC. The enhanced electrochemical performance as a result of the strong SEI layer was evaluated from the *in-situ*-electrochemical impedance study (*in-situ*-EIS). The analysis was continuously recorded for the Li/RG half-cell, and the representative traces of 1st, 5th, 10th, and 25th cycles are given in Figure 5. An increased charge transfer resistance (R_{CT}) value was observed in the initial discharge because of the irreversible capacity loss resulting from electrolyte decomposition, leading to the formation of the SEI layer. However, as the cycle progresses, the R_{CT} value is reduced and is observed to be stable for more than 25 cycles of charge-discharge, which accounts for the stable and robust SEI resulting in superior electrochemical performance. The Nyquist plot and the electrical equivalent circuit corresponding to a higher potential of initial discharge are given in the supplementary part (Figure S6), where the R_{CT} value is found to be 445 Ω . The same circuit diagram applies to the rest of the potentials of the different cycles.

The LIC is a hybrid capacitor consisting of a combination of battery-type electrodes as the anode and a capacitive-type electrode as the cathode. The anode stores energy *via* a faradaic

reaction, whereas a non-faradaic adsorption/desorption is the method of energy storage in the cathode. This work used pre-lithiated RG (LiC_6) as the anode and rGO synthesized from the RG as the cathode. Since two of these electrodes have two different charge-storage mechanisms, the LIC would experience a kinetic mismatch in cycling. Hence, it is necessary to balance the charges between the two electrodes, which could be carried out using the Equation (1). The rGO/pre-lithiated RG (p-RG, LiC_6) full cell was fabricated such that, initially, the Li/RG half-cell was subjected to cycling for two cycles and stopped at the discharged state so that the Li-ions get intercalated into the graphitic layers forming LiC_6 . The cell is then dismantled at this state inside the glove box and is paired with the mass-balanced rGO to get rGO/p-RG LIC. First, the LIC is subjected to cyclic voltammetric studies in the voltage window of 1.3 to 4.3 V at different scan rates ranging from 1–10 mVs⁻¹, as shown in Figure 6a. The cell was also tested at different current densities and various temperature conditions. Figure 6 (b–e) shows the E_{cell} vs. time graph of LIC tested at current densities from 0.1 to 2.5 A g⁻¹ at different temperature conditions (0, 10, 25 and 50 °C). Based on this data, a Ragone plot was also constructed comparing LIC's energy density and power density value for

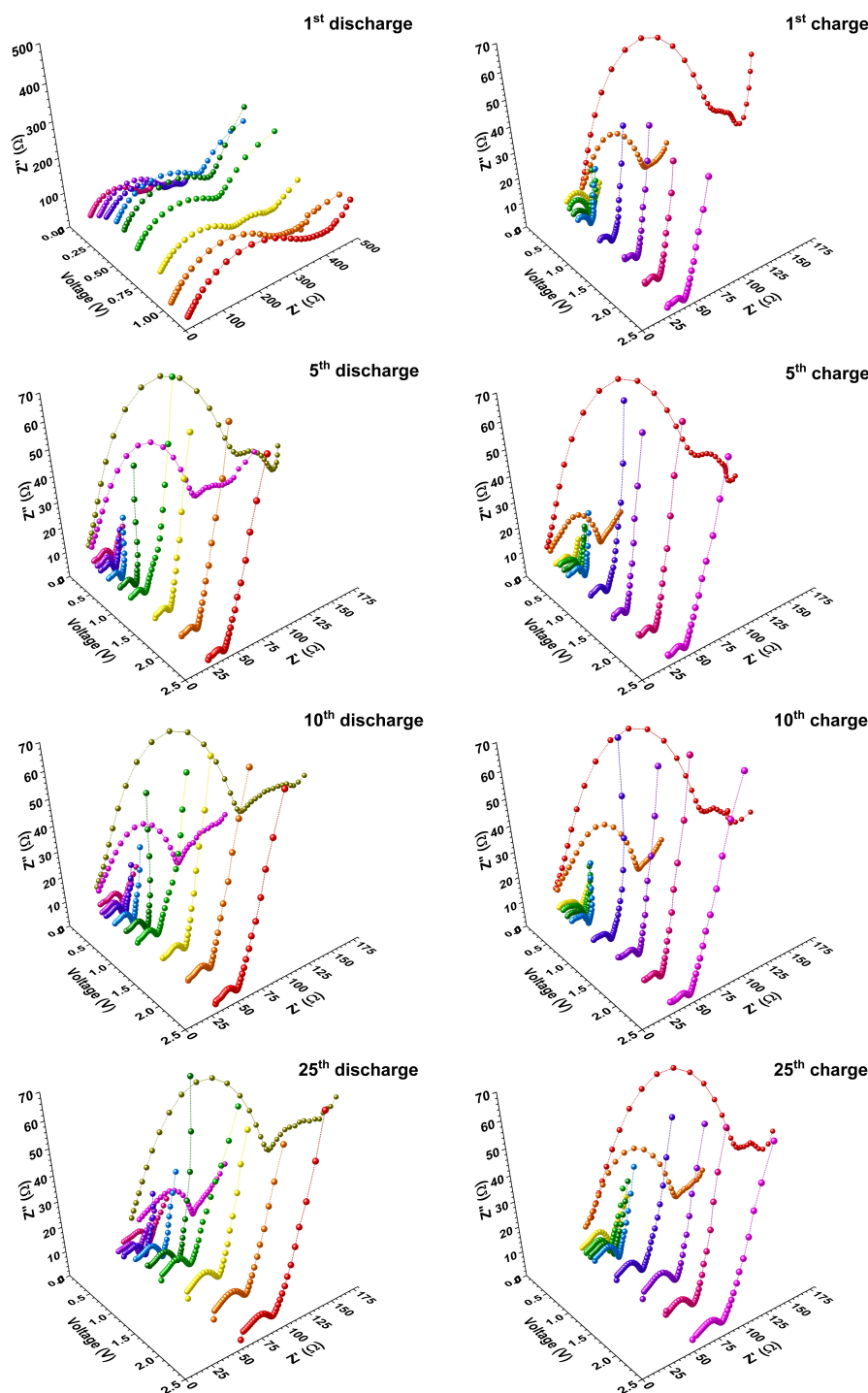


Figure 5. *In-situ* electrochemical impedance spectroscopy (*in-situ*-EIS) profile of Li/RG half-cell with traces of 1st, 5th, 10th, and 25th cycles at different potentials.

these temperatures. The energy and power density values were calculated based on the total active anodic and cathodic masses. Our rGO/p-RG LIC, with an anode: cathode mass loading ratio of 4:8.72 mg, delivered a maximum energy density value of 164.1 Wh kg⁻¹ and a superior power density of 6.9 kW kg⁻¹ at room temperature (Figure 6f).

In addition to the room temperature, the LIC performance was also analyzed at different temperature conditions to

understand the compatibility with various climatic conditions. The LIC exhibited an enhanced performance at all the temperature conditions, and the best was obtained at 50 °C (185.3 Wh kg⁻¹). The superior performance at higher temperatures accounts for the increased electrolyte activity, *i.e.*, ionic conductivity increases with the rise in the temperature. At low temperatures, conversely, the freezing of electrolytes limits the ionic conductivity and, thereby, the overall electrochemical

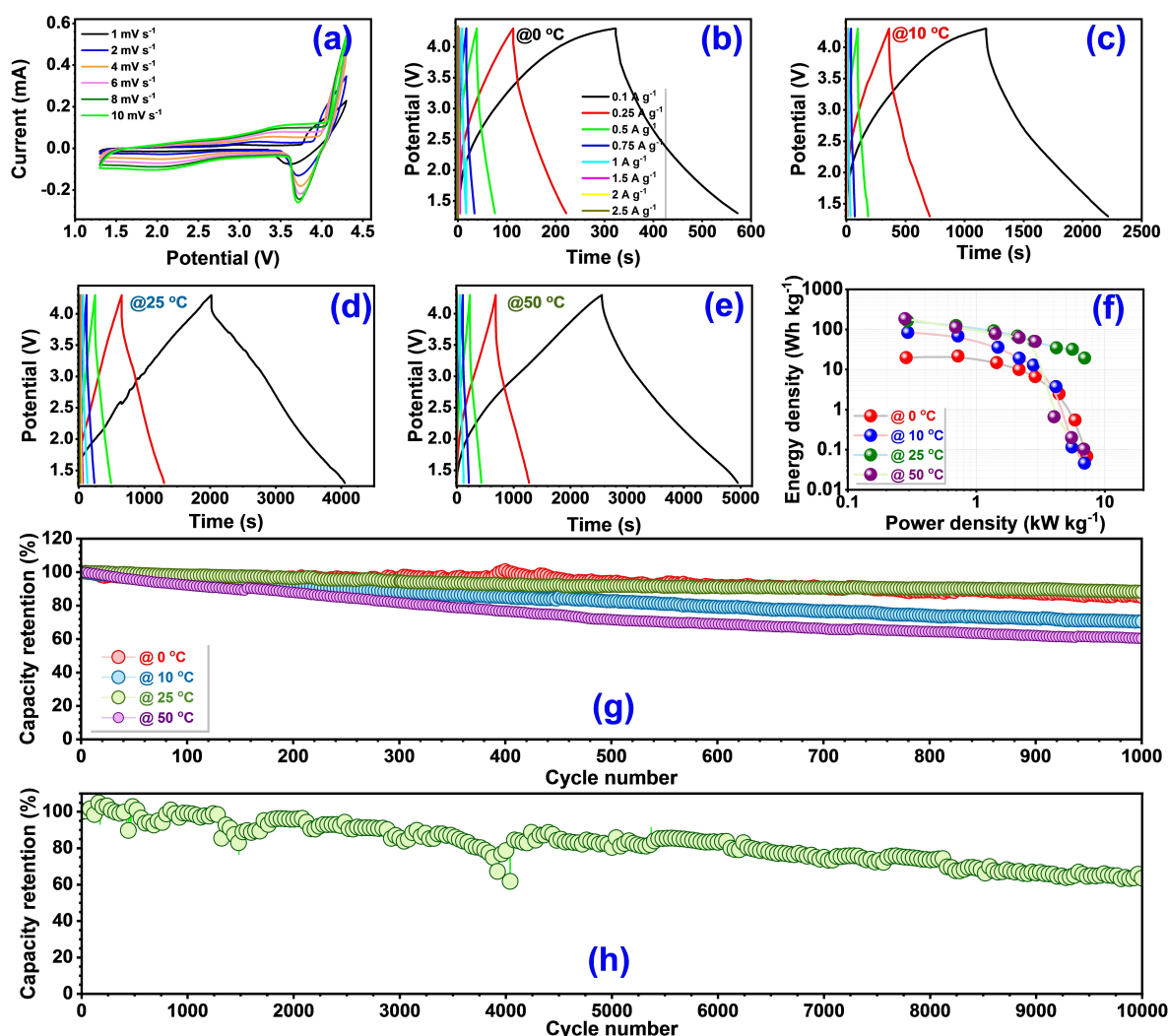


Figure 6. Electrochemical performances of rGO/RG LIC: (a) Cyclic voltammogram at different scan rates, (b–e) Ecell vs. time graph at different temperatures (0, 10, 25, and 50 °C), (f) Ragone plot comparing energy and power density values at different temperatures, (g) long term cycling profile at a current density of 1 A g^{−1} at different temperatures, and (h) long term cycling at room temperature at a current density of 1 A g^{−1}.

performance. The GCD was also performed at these different temperature conditions and is given in Figure 6g with a capacity value normalized to 100% for comparison. All the temperatures exhibited excellent capacity retention even after 1000 cycles. The LIC at 50 °C exhibited a slightly lower retention of capacity after long cycling, which is generally observed in liquid electrolytes due to the inevitable side reactions that can occur at high temperatures. At room temperature, the LIC was also subjected to long-term cycling for more than 10,000 cycles (> 63% retention) at a higher current of 1 A g^{−1} as it is one of the prerequisites for practical applications (Figure 6h). The LIC retained > 83% capacity even after 6000 cycles, which makes it a potential candidate for future practical applications in both direct (graphite, Cu-foil & separator) and converted form (rGO).

Conclusions

In this work, we have developed a novel, scalable, economical, and sustainable method to upcycle graphite, polypropylene separator, and current collector of dead LIBs to active materials for the LICs. The RG was used as the anodic active material and coated over the recycled copper foil current collector. The RG was transformed in rGO using the modified Hummer's method to make it a potential cathode for the LIC. The polypropylene separator was used as such in LIC as it exhibited better performance in physical, mechanical, and electrochemical studies. The electrochemical performance of the recycled and synthesized materials was examined in the half-cell and full-cell configurations. The interfacial properties of the Li/RG half-cell, including the formation of the SEI layer, its stability, robustness, etc., were investigated using *in-situ*-impedance spectroscopic studies. The rGO/p-RG delivered a maximum energy density of 185 Wh kg^{−1} and power density of 6.97 kW kg^{−1} in a rate performance study performed at different temperatures. The

compatibility of LIC to various temperatures (0, 10, 25, and 50 °C) was analyzed by performing GCD at these temperatures. The LIC displayed high capacity retention at all temperatures and long-term cycling at room temperature were excellent as it exhibited high capacity retention after 10,000 cycles. This study paves the way for future research on the development of commercial devices, with most of the components recycled from spent batteries to have a circular economy and sustainable future.

Experimental Section

The spent mobile phone batteries are collected locally for recovery. Initially, the battery is immersed in the NaCl solution overnight for the complete discharge to dismantle it safely. The discharged batteries are washed thoroughly with distilled water, dried, and ensured that the open-circuit voltage is zero. It is cut using cutters and pliers to remove the outer stainless steel/aluminium metallic casing. The anode, polyolefin separator, and cathode are separated manually. Using the following procedures, we have recovered the anodic active material (graphite), the anodic current collector (copper foil), and the separator.

Recovery of Graphite

Two methods were employed for the separation of graphite from the copper foil. One, the graphite is scratched out from the copper foil current collector using the stainless-steel shovel. Two, the anode is immersed in water and is sonicated for a few minutes. The separated graphite is then completely immersed in dimethylformamide (DMF, Sigma Aldrich, >99.8%) solvent and stirred with constant heating at 90 °C for 24 hours to remove the binder (polyvinylidene fluoride, PVdF) stuck with the graphite. After the reaction, the DMF is decanted out, and graphite is dried in the box furnace (Carbolite, UK) at 150 °C for 12 hours. It is again thermally heated in the Ar-atmosphere for 2 hours at 700 °C to get the pure recovered graphite (RG) with well-arranged graphene layers.

Recovery of Copper Foil

A simple sonication method was employed to recover copper foil from the anode. The anode separated from the spent battery is wholly immersed in the distilled water and is sonicated for a few minutes to cast off the graphite stuck to the copper foil. The clean foil thus obtained is washed multiple times with distilled water and then dried for a few hours. After pressing with the calendar press, this copper foil is directly used as the current collector for the LIC. The slurry of the recovered graphite is coated directly over this foil, and the electrode punched out from it is utilised as the anode for our LIC.

Recovery of the Polypropylene Separator

The separator is easily separated from the anodic and cathodic parts. It is cleaned thoroughly using distilled water and sonicated for a few minutes (if required) to remove the electrolyte and active material stuck over it. The clean separator is then dried in the hot air oven for a few hours, and then the circular separator for the cell is punched out from it.

Synthesis of rGO from RG

The GO was prepared from RG by using the modified Hummer's method.^[35] The GO obtained is dispersed in the minimum amount of water. The 10 ml of 2 M NaOH is slowly added to make the pH of the suspension 14. Then, 3 ml of hydrazine hydride is added to it. Finally, it is kept at 90 °C with constant stirring for 2 h to obtain the reduced graphene oxide (rGO).^[32] This rGO is used as the cathode material for the fabrication of LIC.

Material Characterisation

The phase identification and crystallinity of the recovered graphite and synthesized rGO was performed from Powder X-ray diffraction (XRD) measurements using Rigaku Smartlab automated multi-purpose diffractometer (40 kV, 200 mA, $\lambda = 1.5406 \text{ \AA}$) with Cu K α radiation. Both samples were scanned from 10 to 80 °C at a scan rate of 1° min^{-1} . The BET surface area and porosity of RG and rGO were obtained from the automated gas sorption analyser (Autosorb IQ-XR-XR-XR, 3 stat., Viton). Their surface composition was evaluated from the X-ray photoelectron spectroscopy (XPS, Multilab 2000, UK; monochromatic Al K α radiation $h\nu = 1486.6 \text{ eV}$). Raman spectroscopic analysis was performed for both samples using Lab Ram HR800 UV Raman microscope (Horiba Jobin-Yvon, France) with a 515 nm Diode laser as an excitation light source. The morphology, topography, and internal structure of the samples were observed from a field-emission scanning electron microscope (FE-SEM, Gemini 560, Germany). The contact angle of the 1 M LiPF $_6$ in EC: DMC (1:1) electrolyte over the polypropylene separator was measured using Holmarc's contact angle meter (HO-ED-M-01).

Electrochemical Characterizations

Fabrication of RG and rGO Electrodes

The graphite recovered from the dead batteries is coated over the recovered copper foil. The slurry for coating was prepared and coated over the foil using the doctor blade apparatus. The active material (RG), conductive carbon (acetylene black, AB) and binder (PVdF) are taken in the 80:10:10 (wt%) ratio and coated in 40 mm thickness. Initially, the PVdF is dissolved in the 1-Methyl-2-pyrrolidinone (NMP, anhydrous, Sigma Aldrich, >99.5%) solvent by continuous stirring for 30 min. Then, the AB and RG are weighed and added to it, respectively. After stirring for overnight time, a homogenous slurry is obtained. This slurry is cast onto the recovered copper foil and dried in the hot air oven at 65 °C for 4 h. The coating is then pressed using a calendar roller machine, and the 12 mm electrodes are punched out of it for the electrochemical study. The electrodes are stored in a dry cabinet until the fabrication of the cells. In contrast, a simple hand-made method was employed to fabricate the rGO electrodes. A thin free-standing film was made by mixing the rGO, AB, and teflonized acetylene black (TAB-2) binder in a mortar pestle using ethanol as the solvent. These constituents mixed are taken in the 8:1:1 ratio. The obtained film was then pressed onto a 14 mm stainless steel mesh (Good-fellow, UK) in a pellet maker using the hydraulic press (Specac, UK).

Fabrication and Testing of Ion-Blocking Cell

The ion-blocking cell was fabricated using the CR-2016 type coin cell. A stainless-steel disc (SS disk) of 16 mm diameter was used as the electrode, which blocks the Li $^+$ transport but provides electronic conductivity. The cell was fabricated so that the SS disk was placed over the cathode cap, covered with two circular sheets

of electrolyte-soaked PP separator (fresh/recycled), then with the SS disk over it and finally crimped after covering with the anode cap.

The ion-blocking cell was fabricated to calculate the conductance and activation energy of the electrolyte using the Arrhenius plot. For that, electrochemical impedance spectroscopy (EIS) was run from 10 kHz to 10 MHz frequency with an applied ac amplitude of 10 mV at different temperatures. The cells were tested at different temperatures by inserting them into an environmental chamber (Espec SU-242 bench-top type thermal chamber) and adjusting the temperatures before running the EIS.

Fabrication and Testing of Li/Li Symmetric Cell

The Li/Li symmetric non-blocking cell was fabricated using the same CR-2016 type coin cell for the galvanostatic charge-discharge studies. The circular 14 mm diameter Li was placed over the cathode cap, on which the two separators (fresh/recycled) were kept and then covered with another Li metal disc. A total of 75 μL of electrolyte was added in different steps to ensure proper wetting of the separator and enhance the stability in Li stripping-plating in the test. The fabricated cell was subjected to charge-discharge at a constant current of 0.1 mA cm^{-2} , keeping 0.1 mAh cm^{-2} as the capacity limit (separator area = 2.985 cm^2 , radius of 0.975 cm).

Fabrication and Testing of Li/Stainless-Steel (SS) Asymmetric Cell

The asymmetric cell was fabricated for the linear sweep voltammetry (LSV) studies using the same coin-cell setup. Here, one of the electrodes is an SS disk, and the other is Li metal. A similar method of fabrication, as above, was adopted for this asymmetric cell fabrication. The Li metal disc was placed over the cathode cap, followed by covering it with two sheets of electrolyte-soaked separators (fresh/recycled), and then the SS disk was carefully placed over it before crimping the cell. The fabricated cell was tested from open circuit potential (OCV) to 6 V vs. Li at a scan rate of 0.1 mVs^{-1} .

Half-Cell and Full-Cell Analysis

All the half-cells and full-cells were fabricated inside the argon-filled glove box (MBraun, Germany) workstation, with O_2 and H_2O levels less than 0.1 ppm, using the CR2016-type coin cell. The electrodes were dried inside a vacuum oven at 75 $^\circ\text{C}$ for at least 4 h before being inserted into the glove box. The half cells are fabricated such that initially, the electrodes are placed over the cathode cap, followed by the recovered polypropylene separator (2 nos). Then, the Li metal disk of 14 mm diameter is placed over the electrolyte-wetted separator before crimping the cell. The electrolyte used in the cell is a commercially available 1 M LiPF_6 salt dissolved in ethylene carbonate (EC) and dimethyl carbonate (DMC) solvent in a 1:1 ratio. All the fabricated cells were subjected to electrochemical testing using a biological battery tester (BCS-805, France) and Solartron (UK).

Acknowledgments

The authors acknowledge Dr. Maheshwar Reddy Gopu for recording the contact angle measurements. YSL acknowledges the financial support from the National Research Foundation of Korea (NRF) grant funded by the Korean government (Ministry of Science, ICT&Future Planning) (RS-2023-00208361). VA

acknowledges financial support from the Anusandhan National Research Foundation (ANRF) through Swarnajayanti Fellowship (SB/SJF/2020–21/12) and Waste Management Technologies (DST/TDT/WMT/Power Ind. Waste/2021/01) by Department of Science and Technology, Govt. of India.

Conflict of Interests

The authors declare no conflict of interest.

Data Availability Statement

The data that support the findings of this study are available from the corresponding author upon reasonable request.

Keywords: Li-ion capacitor · Spent li-ion battery recycling · Anode · Cathode · Separator · Current collectors

- [1] M. Li, J. Lu, Z. Chen, K. Amine, *Adv. Mater.* **2018**, *30*, 1800561.
- [2] A. Jagadale, X. Zhou, R. Xiong, D. P. Dubal, J. Xu, S. Yang, *Energy Storage Mater.* **2019**, *19*, 314–329.
- [3] C. W. Babbitt, *Clean Technol. Environ. Policy* **2020**, *22*, 1213–1214.
- [4] S. Natarajan, R. M. Bhattarai, M. S. P. Sudhakaran, Y. S. Mok, S. J. Kim, *J. Power Sources* **2023**, *577*, 233170.
- [5] S. Natarajan, V. Aravindan, *Adv. Energy Mater.* **2020**, *10*, 2002238.
- [6] Z. J. Baum, R. E. Bird, X. Yu, J. Ma, *ACS Energy Lett.* **2022**, *7*, 712–719.
- [7] O. Velázquez-Martínez, J. Valio, A. Santasalo-Aarnio, M. Reuter, R. Serna-Guerrero, *Batteries* **2019**, *5*, 5–7.
- [8] S. Natarajan, M. Akshay, V. Aravindan, *Adv. Sustain. Syst.* **2022**, *6*, 2100432.
- [9] J. Neumann, M. Petranikova, M. Meeus, J. D. Gamarra, R. Younesi, M. Winter, S. Nowak, *Adv. Energy Mater.* **2022**, *12*, 2102917.
- [10] M. T. Islam, U. Iyer-Raniga, *Recycling* **2022**, *7*, DOI: 10.3390/recycling7030033.
- [11] X. Zeng, J. Li, N. Singh, *Crit. Rev. Environ. Sci. Technol.* **2014**, *44*, 1129–1165.
- [12] Y. Wang, C. Yin, Z. Song, Q. Wang, Y. Lan, J. Luo, L. Bo, Z. Yue, F. Sun, X. Li, *Materials (Basel)* **2019**, *12*, 3125 DOI: 10.3390/ma12193125.
- [13] X. Ma, M. Chen, B. Chen, Z. Meng, Y. Wang, *ACS Sustain. Chem. Eng.* **2019**, *7*, 19732–19738.
- [14] M. L. Divya, S. Natarajan, V. Aravindan, *Batter. & Supercaps* **2022**, *5*, e202200046.
- [15] C. Badenhorst, I. Kuzniarska-Biernacka, A. Guedes, E. Mousa, V. Ramos, G. Rollinson, G. Ye, B. Valentim, *Recycling* **2023**, *8*, 1–18.
- [16] S. Natarajan, A. B. Boricha, H. C. Bajaj, *Waste Manag.* **2018**, *77*, 455–465.
- [17] S. Natarajan, M. L. Divya, V. Aravindan, *J. Energy Chem.* **2022**, *71*, 351–369.
- [18] S.-J. Han, L. Xu, C. Chen, Z.-Y. Wang, M.-L. Fu, B. Yuan, *Sep. Purif. Technol.* **2024**, *330*, 125289.
- [19] S. Natarajan, R. M. Bhattarai, M. S. P. Sudhakaran, Y. S. Mok, S. J. Kim, *J. Power Sources* **2023**, *577*, 233170.
- [20] S. Natarajan, K. Subramanyan, R. B. Dhanalakshmi, A. M. Stephan, V. Aravindan, *Batter. Supercaps* **2020**, *3*, 581–586.
- [21] K. Subramanyan, S. Jyothilakshmi, M. Ulaganathan, Y. S. Lee, V. Aravindan, *Carbon N. Y.* **2024**, *216*, 118525.
- [22] S. Natarajan, K. Subramanyan, R. B. Dhanalakshmi, A. M. Stephan, V. Aravindan, *Batter. and Supercaps* **2020**, *3*, 581–586.
- [23] M. Akshay, K. Subramanyan, M. L. Divya, Y.-S. Lee, V. Aravindan, *Adv. Mater. Technol.* **2022**, *7*, 2200423.
- [24] K. Subramanyan, M. Akshay, Y.-S. Lee, V. Aravindan, *Adv. Mater. Technol.* **2022**, *7*, 2200399.
- [25] M. Akshay, K. Subramanyan, Y.-S. Lee, V. Aravindan, *Sustain. Mater. Technol.* **2023**, *36*, e00603.
- [26] U. Bhattacharjee, M. Bhar, S. Bhowmik, S. K. Martha, *Sustain. Energy Fuels* **2023**, *7*, 2104–2116.
- [27] S. Natarajan, M. Akshay, V. Aravindan, *Small* **2023**, *19*, 2206226..

- [28] S. Yuan, Q. Lai, X. Duan, Q. Wang, *J. Energy Storage* **2023**, *61*, 106716.
- [29] C. Li, Y. An, L. Wang, K. Wang, X. Sun, H. Zhang, X. Zhang, Y. Ma, *Chem. Eng. J.* **2024**, *485*, 149880.
- [30] W. Liu, Y. An, L. Wang, T. Hu, C. Li, Y. Xu, K. Wang, X. Sun, H. Zhang, X. Zhang, Y. Ma, *J. Energy Chem.* **2023**, *80*, 68–76.
- [31] L. Wang, X. Zhang, C. Li, Y. Xu, Y. An, W. Liu, T. Hu, S. Yi, K. Wang, X. Sun, Y. Gong, Z.-S. Wu, Y. Ma, *Chem. Eng. J.* **2023**, *468*, 143507.
- [32] A. Viswanathan, A. N. Shetty, *Electrochim. Acta* **2017**, *257*, 483–493.
- [33] R. Al-Gaashani, A. Najjar, Y. Zakaria, S. Mansour, M. A. Atieh, *Ceram. Int.* **2019**, *45*, 14439–14448.
- [34] Z. Chen, D. Bresser, J. Asenbauer, T. Eisenmann, M. Kuenzel, Z. Chen, D. Bresser, *Sustain. Energy Fuels* **2020**, *4*, 5387–5416 DOI: 10.1039/d0se00175a.
- [35] N. I. Zaaba, K. L. Foo, U. Hashim, S. J. Tan, W.-W. Liu, C. H. Voon, *Procedia Eng.* **2017**, *184*, 469–477.

Manuscript received: February 29, 2024
Revised manuscript received: April 1, 2024
Accepted manuscript online: July 23, 2024
Version of record online: October 10, 2024